

Primary Quantum Yields of Photodecomposition of Acetone in Air under Tropospheric Conditions

Edward P. Gardner,* Ranmali D. Wijayaratne, and Jack G. Calvert

National Center for Atmospheric Research,[†] Boulder, Colorado 80307 (Received: February 24, 1984)

The primary quantum yields of acetone loss and formation of the products CO₂, CO, CH₃OH, and CH₂O have been measured for the photolysis of dilute acetone mixtures in synthetic air. Experiments were carried out by using several wavelength regions for excitation (λ_{max} , 313, 299, 290, and 279 nm), with a range of temperatures (-1 to 28 °C) and pressures of air (25-745 torr) which are characteristic of tropospheric conditions. The quantum yields of acetone photodecomposition (to form CH₃CO and CH₃ radicals) decrease with increasing air pressure (25-350 torr), but about 7% of the decomposition of excited acetone molecules is independent of the pressure in the range 350-745 torr. The estimated apparent first-order photochemical decay constants for acetone in the troposphere are much smaller than those for CH₂O and CH₃CHO.

Introduction

Acetone is among a number of organic compounds which have been identified as hazardous air pollutants by the U.S. Environmental Protection Agency. Of special concern is the potential buildup of the concentrations of these species in the ambient atmosphere to which the population is exposed. It is clear from recent data of Penkett that rather large concentrations of acetone are observed even in the relatively clean Atlantic air (e.g., 408-627 ppt).¹ Penkett has suggested that direct photolysis is the main removal mechanism for acetone and that the lifetime of acetone in the troposphere lies somewhere between that for C₂Cl₄ and CHCl₃. Previous studies of acetone photooxidation allow no definitive conclusion to be made in this regard.

Acetone photochemistry has been studied for over half a century, and many of the details of its mechanism have been well established for the oxygen-free system.^{2,3} Hence, evidence is strong that the major overall chemical decomposition mode at longer wavelengths is described by process I.



In an oxygen-free, gaseous mixture or at low O₂ pressures, reaction I occurs largely from the first excited triplet state of acetone when excitation occurs in the long-wavelength region (313 nm) of the acetone absorption spectrum. Obviously, if reaction I occurs in air, then the free-radical fragments (CH₃ and CH₃CO) will react readily with oxygen to form various oxidation products. However, it is not known to what extent the triplet state reacts directly with oxygen to yield final products and/or the extent of quenching of the excited triplet species by O₂ without product formation. Moreover, studies for the very reaction conditions most important for tropospheric considerations, very dilute acetone mixtures in air at tropospheric pressures (25-760 torr) and temperatures (≤ 25 °C), have not been carried out to date. Most previous studies of acetone photooxidation have been made under conditions of relatively high acetone pressure (commonly 20-150 torr), low oxygen pressure (usually less than 1 torr), and relatively high temperature (120-225 °C).⁴⁻⁹ The few photooxidation studies which have been made at more realistic atmospheric temperatures (about 25 °C) utilized either relatively large acetone concentrations or very low oxygen concentrations.¹⁰⁻¹⁶ In such studies the secondary reactions of the free radicals formed in the primary photochemical processes involved reactant acetone molecules. This complication obscures the nature and the quantum efficiency of the primary processes and obviates any use of the results to extrapolate to atmospheric conditions.

The experiments reported here were designed to simulate closely the conditions commonly encountered in the troposphere. Very small concentrations of acetone were photolyzed at selected wavelength regions, pressures of synthetic air, and salient tro-

spheric temperatures. The results provide quantitative information on the primary quantum yields of acetone photooxidation and therefore provide the basis for the first realistic estimates of the photochemical decay rate constants for acetone under tropospheric conditions.

Experimental Section

Central to the experimental apparatus is the large reaction cell and associated optical system used to generate the excitation beam and to monitor its intensity (illustrated in Figure 1). The reaction cell (internal optical path, 155.8 cm; volume, 4713 cm³) was fitted with Suprasil windows sealed onto the ground end of the inner glass sleeve. The sleeve, ring-sealed into a 75 O-ring joint, allowed the windows to protrude into the reaction cell so that the window temperatures matched those of the cell itself. The desired cell temperature was maintained by the circulation of the temperature-controlled supply of an ethylene glycol-water mixture through the double-wall structure of the cell. The desired band of wavelengths (centered at 313-, 299-, 290-, and 279-nm regions) for each series of photochemical studies was determined by the choice of narrow-band filters placed between the cell and the ultraviolet lamp (Osram HBO 500 W/2). The relative intensity of the light exiting the cell was monitored continuously by a combination of a photomultiplier (RCA 8575), scaler-timer, and a digital pulse-height analyzer. The entire optical train, including the lamp housing, filter assembly, cell, and photomultiplier unit, was held in alignment through O-ring joints (see Figure 1), and nitrogen gas was used to purge continuously the noncell components of the optical path.

Gas mixtures were prepared in a multifunctional gas-handling vacuum system attached to the cell. This provided storage, high

(1) S. A. Penkett in "Atmospheric Chemistry", Dahlem Conference, E. D. Goldberg, Ed., Springer-Verlag, Berlin, 1982, pp 329-55.

(2) For a current review of the photophysical aspects of the extensive work on acetone photoprocesses see E. K. C. Lee and R. S. Lewis, *Adv. Photochem.*, **12**, 1 (1980).

(3) W. A. Noyes, Jr., G. B. Porter, and J. E. Jolley, *Chem. Revs.*, **56**, 49 (1956).

(4) F. B. Marcotte and W. A. Noyes, Jr., *J. Am. Chem. Soc.*, **74**, 783 (1952).

(5) D. E. Hoare, *Trans. Faraday Soc.*, **49**, 1292 (1953).

(6) R. R. Hetz, *J. Am. Chem. Soc.*, **75**, 5810 (1953).

(7) M. I., Christie, *J. Am. Chem. Soc.*, **76**, 1979 (1954).

(8) J. R. Dunn and K. O. Kutschke, *Can. J. Chem.*, **35**, 421 (1958).

(9) J. Brown, N. T. Mitchell, and G. R. Martin, *Proc. Chem. Soc.*, 115 (1960).

(10) R. Srinivasan and W. A. Noyes, Jr., *J. Am. Chem. Soc.*, **82**, 5591 (1960).

(11) A. D. Osborne, J. N. Pitts, Jr., and S. L. Fowler, *J. Phys. Chem.*, **65**, 1622 (1961).

(12) A. D. Kirk and G. B. Porter, *J. Phys. Chem.*, **66**, 556 (1962).

(13) J. Caldwell and D. E. Hoare, *J. Am. Chem. Soc.*, **84**, 3990 (1962).

(14) G. S. Pearson, *J. Phys. Chem.*, **67**, 1686 (1963).

(15) R. Srinivasan, *J. Phys. Chem.*, **68**, 1997 (1964).

(16) H. S. Johnston and J. Heicklen, *J. Am. Chem. Soc.*, **86**, 4249 (1964).

[†]The National Center for Atmospheric Research is sponsored by the National Science Foundation.

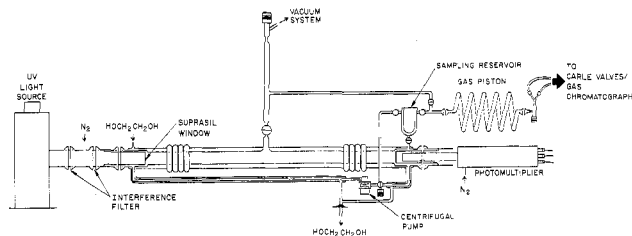


Figure 1. Photochemical reaction cell and the associated components of the optical train.

vacuum/reference, gas measurement, calibration, mixture preparation, and reactant purification. Gas mixtures were prepared by using calibrated volumes and a bank of manometers (MKS Baratron capacitance). The homogeneity of the mixtures was assured through the use of a centrifugal pump in series with the cell (Figure 1) driven by an external rotating magnet. Following a photochemical experiment, the gas mixture was diverted from the cell into the Dewar-sampling reservoir shown in the Figure 1. The contents of this reservoir could be sealed off from the cell, fractionated, and/or expanded into a "gas piston" which led to the analysis system. The volumes of the cell and all other parts of the system were determined accurately so that the amounts of materials employed at each stage of the experiments were known.

The absolute light intensities were measured by employing two chemical actinometers. Small pressures of acetone or azomethane were introduced, the fraction of the incident light which was absorbed was measured, and photolysis was carried out to a few percent conversion. When acetone was employed as the actinometer, the cell temperature was regulated to 120 °C, and the CO product ($\Phi_{\text{CO}} = 1.00$) was determined. With azomethane the photolyses were conducted at 25 °C and the N_2 product ($\Phi_{\text{N}_2} = 1.00$) was determined.

In preparation for each photolysis of a mixture of acetone in synthetic air, the reaction cell was heated to about 100 °C and evacuated well by using the high-vacuum system. The cell was then cooled to 25 °C and filled with a synthetic air mixture, without acetone, and the contents were circulated for about 1 h. After circulation, the mixture was sampled and analyzed chromatographically to search for possible contaminants either as retained products from a previous run or as impurities in the reactant gases. When assured of no contamination, we sequentially reevacuated the cell, equilibrated the lamp, and determined the intensity of the light transmitted through the empty cell. The cell was then filled with an accurately measured amount of acetone (about 0.36 torr) and krypton ([acetone]/456), followed by O_2 and N_2 (ratio 1 to 4) at the desired pressures (20–745 torr). The accurately measured krypton gas served as an internal standard and provided a convenient reference for normalization of amounts of individual components in the reaction mixture. The cell contents were allowed to circulate for about 30 min to ensure uniform mixing, followed by expansion into and circulation through the reservoir/sampling chamber. After an additional 15 min of gas circulation, the sampling chamber was sealed from the photolysis cell, and the circulating reaction mixture was redirected to the normal flow path through the cell. The aliquot of the unphotolyzed reactant mixture held in the reservoir/sample chamber served as a control which was analyzed ahead of the product mixture following the photolysis.

The absorbed light intensities ($\text{quanta cm}^{-2} \text{s}^{-1}$) were in the following ranges: $(0.86\text{--}1.12) \times 10^{11}$ at 313 nm; $(8.9\text{--}9.0) \times 10^{11}$ at 299 nm; $(1.42\text{--}1.44) \times 10^{11}$ at 290 nm; and $(3.0\text{--}3.6) \times 10^{11}$ at 279 nm. The photolysis times (240–1455 min) were controlled to restrict the fraction of the acetone decomposed to a few percent. Analyses following the photolysis were initiated by diverting the flow of the circulating reaction mixture through the reservoir/sample chamber. The chamber was then sealed from the reaction cell and its contents were cryogenically fractionated, if desired, or expanded directly into the gas piston (spiral tube, 118 cm long, 2.5 cm in diameter). Helium gas at 800 torr was then introduced

to the piston to compress the gas sample into a plug which was received by a 3.0- cm^3 stainless steel sample loop. The loop was automatically evacuated between sampling cycles. A microprocessor was employed to operate, on a programmed sampling schedule, four Carle, microvolume, gas sampling valves which loaded aliquots of the reaction mixture onto the gas-chromatographic columns. The GC (Varian, Model 2700) was equipped with both flame ionization and thermal conductivity detectors. Two columns were used: (1) Porapak P/Q (mixture), 80/100 mesh, 75 °C isothermal, 57 $\text{cm}^3 \text{min}^{-1}$ He carrier gas, 3.0 m \times 2.6 mm i.d.; (2) molecular sieve 13X, 80/100 mesh, 50 and 75 °C isothermal, same He flow and column size. The detectors were held at 200 °C for all analyses. The Porapak P/Q column effectively separated the photolysis products CO_2 , CH_2O , H_2O , CH_3OH and the residual reactant CH_3COCH_3 . The molecular sieve had an excellent resolution of CO , O_2 , N_2 and the $\text{C}_1\text{--C}_3$ hydrocarbons.

A quantitative mass spectrometer (CEC 21-104) was employed to obtain precise measurement of the H_2 and CO products in additional runs at pressures of added oxygen between 5 and 10 torr. Argon was used as the internal standard in these experiments. Cryogenic separation of volatile and nonvolatile (at $\sim 77 \text{ K}$) constituents of the photolyzed mixture was performed on the vacuum line-inlet system of the mass spectrometer. Products identified by gas chromatography were confirmed on the mass spectrometer after collecting the substance upon its elution from the GC column.

Results

The photodecomposition of dilute acetone mixtures in air was studied at selected wavelength regions, temperatures, and pressures of added synthetic air in order to determine the photochemical behavior of acetone in the troposphere. The experimental conditions and the quantum yields obtained in 40 different experiments are summarized in Table I. Reported here are quantum yields of acetone loss and formation of the products CO_2 , CO , CH_3OH , and CH_2O . Water and hydrogen were also observed among the products. Both are probably secondary products. Water is undoubtedly formed from some of the unstable products such as H_2O_2 , $\text{HO}_2\text{CH}_2\text{OH}$, and $\text{CH}_3\text{O}_2\text{H}$. However, it is a ubiquitous compound in glass systems, readily desorbed from the interior structure of the cell walls through slow diffusional processes which may occur during a long experiment. Although some of the water observed must have been derived from reaction products, an unknown amount of water was contributed inevitably from trivial glass wall sources unrelated to the homogeneous reactions of acetone. Because of the uncertainties regarding the sources of water, the quantum yields of water formation are not reported. The expected products of acetone photooxidation, H_2O_2 , $\text{CH}_3\text{O}_2\text{H}$, and HCO_2H , could not be determined quantitatively by using the analytical methods employed. Hydrogen was observed as a product but could not be measured accurately by gas chromatography with the employed conditions of high pressures of added air. A separate set of experiments utilizing low pressures of added O_2 and quantitative analysis by mass spectrometry provided accurate measurement of H_2 (and CO) yields for these conditions.

Discussion

Mechanism of the Primary Photodecomposition Processes in Acetone Photooxidation. The experimental results provide new information of importance to understanding the mechanism of acetone photooxidation under tropospheric conditions. In this section, we consider the results which elucidate the nature of the primary photodecomposition processes in acetone photooxidation.

In a given experiment the quantum yields of acetone loss (Φ_{A}) and CO_2 formation (Φ_{CO_2}) are equal within the experimental error; the average ratio of $\Phi_{\text{A}}/\Phi_{\text{CO}_2}$ for 40 different experiments is 1.02 ± 0.03 . This near equality of Φ_{A} and Φ_{CO_2} is maintained for all employed conditions of pressure, temperature, and wavelength. The simplest, favored explanation of this observation is that rupture of the $\text{CH}_3\text{CO--CH}_3$ bond constitutes the primary dissociation

TABLE I: Summary of Experimental Conditions and Quantum Yield Results from Acetone Photodecomposition in Simulated Air Mixtures

run no.	reactant concn, molecules cm ⁻³			temp, °C	quantum yield				
	[CH ₃ COCH ₃]	10 ⁻¹⁸ [O ₂]	10 ⁻¹⁹ [N ₂]		CH ₃ COCH ₃ (loss)	CO ₂	CO	CH ₃ OH	CH ₂ O
(a) Excitation (λ _{max}), 313 nm									
1	1.14	4.767	1.923	27.6	0.0799	0.0780	a	0.0186	0.0247
2	1.15	2.451	0.969	26.4	0.0780	0.0755	0.0169	0.0178	0.0243
3	1.15	1.200	0.485	25.9	0.0878	0.0896	0.0259	0.0210	0.0380
4	1.15	0.604	0.244	25.5	0.1379	0.1262	0.0301	0.0239	0.0308
5	1.15	0.290	0.123	26.2	0.1290	0.1274	0.0316	0.0297	0.0344
6	1.16	3.498	1.415	25.2	0.0739	0.0722	a	0.0184	0.0245
7	1.15	0.770	0.310	26.4	0.1090	0.1038	0.0294	0.0247	0.0303
8	1.15	1.075	0.432	24.8	0.1113	0.1059	0.0260	0.0213	0.0277
9	1.15	3.487	1.409	27.0	0.0767	0.0764	a	0.0179	0.0243
10	1.15	4.178	1.690	27.2	0.0805	0.0756	a	0.0182	0.0244
11	1.15	0.917	0.370	26.2	0.0991	0.0944	0.0275	0.0229	0.0293
12	1.15	4.546	1.838	26.5	0.0757	0.0745	a	0.0176	0.0246
13	1.14	0.159	0.0696	25.6	0.1603	0.1493	0.0355	0.0315	0.0356
14	1.14	1.823	0.734	25.6	0.0793	0.0811	0.0209	0.0186	0.0242
15	1.15	1.210	0.000	25.1	0.0827	0.0823	0.0323	0.0185	0.0304
16	1.16	3.226	0.000	23.2	0.0751	0.0770	0.0168	0.0168	0.0230
17	1.15	17.716	0.000	22.7	0.0736	0.0752	a	0.0162	0.0215
18	1.14	0.804	0.000	24.9	0.1140	0.1081	0.0358	0.0224	0.0419
19	1.15	2.031	0.000	25.1	0.0768	0.0805	0.0246	0.0180	0.0286
(b) Excitation (λ _{max}), 299 nm									
20	1.15	1.719	0.695	24.9	0.0788	0.0769	0.0211	0.0248	0.0215
21	1.15	0.273	0.115	24.9	0.1276	0.1306	0.0283	0.0565	0.0097
22	1.16	0.956	0.386	23.6	0.1037	0.1011	0.0262	0.0306	0.0179
23	1.16	2.499	1.000	23.8	0.0799	0.0778	0.0154	0.0219	0.0207
24	1.16	3.549	1.436	24.0	0.0775	0.0763	a	0.0202	0.0235
25	1.16	4.440	1.787	24.2	0.0752	0.0762	a	0.0194	0.0230
26	1.14	0.160	0.0696	0.1	0.1710	0.1705	0.0237	0.0916	0.0463
27	1.15	0.849	0.341	-0.3	0.1063	0.1027	0.0023	0.0339	0.0332
28	1.15	2.641	1.057	-0.4	0.0781	0.0732	a	0.0176	0.0306
29	1.15	0.275	0.110	-1.1	0.1449	0.1436	0.0104	0.0723	0.0412
30	1.15	1.342	0.537	-0.8	0.0908	0.0866	a	0.0256	0.0321
(c) Excitation (λ _{max}), 290 nm									
31	1.17	0.203	0.0870	23.8	0.1387	0.1365	0.0263	0.0642	0.0428
32	1.16	0.826	0.332	24.4	0.1002	0.1051	0.0239	0.0338	0.0410
33	1.15	1.628	0.660	25.0	0.0864	0.0833	0.0202	0.0251	0.0376
34	1.16	4.064	1.635	25.2	0.0801	0.0799	a	0.0195	0.0354
(d) Excitation (λ _{max}), 279 nm									
35	1.15	2.401	0.971	25.6	0.0785	0.0787	0.0151	0.0222	0.0468
36	1.15	4.652	1.874	25.0	0.0769	0.0736	a	0.0191	0.0471
37	1.15	0.157	0.0695	24.9	0.1554	0.1480	0.0222	0.0711	0.0511
38	1.14	3.614	1.449	25.7	0.0815	0.0790	a	0.0200	0.0454
39	1.15	0.785	0.314	24.7	0.1024	0.0968	0.0211	0.0349	0.0548
40	1.16	1.445	0.583	23.8	0.0821	0.0785	0.0196	0.0262	0.0519

^a Could not be determined because of high O₂ concentration in these runs.

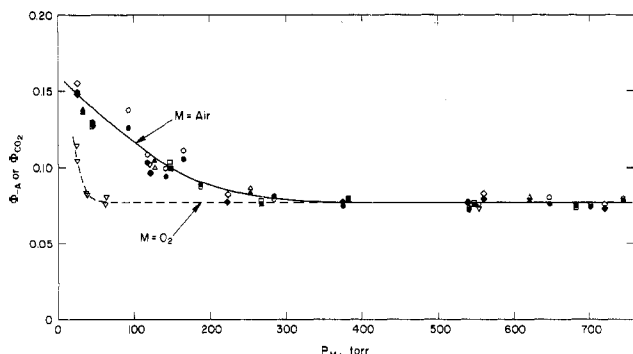


Figure 2. Plot of the quantum yields of acetone loss (Φ_A), shown as open symbols, or CO₂ production (Φ_{CO_2}), closed symbols, vs. the pressure of added air (solid curve) or oxygen (dashed curve); wavelength of excitation: 313 nm, circles; 299 nm, squares; 290 nm, triangles; 279 nm, diamonds.

process in acetone photolysis, and each CH₃CO radical fragment leads ultimately to CO₂. For our conditions of high O₂ pressures, the CH₃CO and CH₃ radicals formed will always react to generate CH₃COO₂ and CH₃O₂ radicals, respectively. The attack of these peroxy radicals on reactant acetone or other product molecules

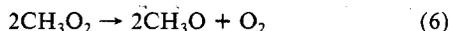
will not occur significantly for the employed conditions of relatively low temperature and low acetone concentration. Therefore, radical-radical interactions should determine the ultimate fate of these species. To satisfy the experimentally observed equality, $\Phi_A = \Phi_{CO_2}$, one molecule of CO₂ product must form for every peroxyacyl radical created. The following reaction sequence is consistent with these observations:



The CH₃CO₂ radical lifetime should be very short, and CO₂ generation would result from its exclusive, rapid decay in reaction 5. CH₃O₂ radicals will also react in the well-known reactions



6 and 7. Theoretically, reaction 8 could provide an alternative





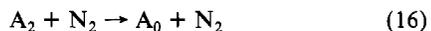
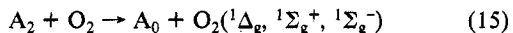
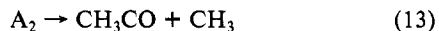
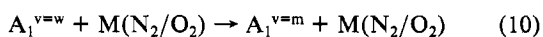
reaction channel to reaction 4 by analogy with reactions 6 and 7. However, since $\text{CH}_3\text{CO}_2\text{H}$ is not a major product ($0.001 < \Phi < 0.01$) and given the observed equality, $\Phi_{-\text{A}} = \Phi_{\text{CO}_2}$, we conclude that $k_8 \ll k_4$.

Therefore with the mechanism outlined, the equality of the quantum yields of CO_2 formation and acetone loss in a given experiment reflects the occurrence of reactions 1–5 following the acetone dissociation in the primary photochemical process I. Accordingly, the removal of additional acetone molecules through reactions with the subsequent radicals or products formed in the system appears to be unimportant for our conditions. This interpretation, completely consistent with theoretical expectations for the employed dilute reacting mixtures, suggests that the primary quantum yields of photodissociation of acetone in dilute air mixtures (temperature $\leq 25^\circ\text{C}$) can be estimated from either $\Phi_{-\text{A}}$ or Φ_{CO_2} . Other observations from the present results confirm this conclusion.

The quantum yields of acetone loss and the quantum yields of product formation all show a significant decrease with increasing pressures of air in experiments from 25 to about 375 torr; see Figure 2 (solid curve). However, as the air pressure is increased from 375 to 750 torr, little, if any, further decrease in quantum yields is observed. Furthermore, results from experiments with all four wavelength regions show the same magnitude of the quenching effect; i.e., within the experimental error, the quantum yields for experiments at the same pressure are equal regardless of the wavelength region of excitation (313–279 nm).

The results at high pressures of air demonstrate that about 7.7% of the excited molecules of acetone are not quenched even at pressures of 1 atm of air. Either the excited acetone molecules dissociate directly to free-radical products after absorption of a quantum or, alternatively, they undergo chemical reaction with molecular oxygen. The first alternative is favored by other evidence as will be discussed later in this section.

Note in Figure 2 (dashed curve) that when O_2 is used as the quencher gas in place of the synthetic air mixture at the same total pressure, a much greater suppression of the quantum yields is observed, although the limiting quantum yield at high pressures is the same for air or pure oxygen within the experimental error. A relatively simple mechanism which can rationalize the results is the following:



Here A_0 represents the ground-state acetone molecule; $\text{A}_1^{v=w}$ is the first excited singlet molecule formed with vibrational energy which presumably increases with energy of the absorbed light quantum in the excitation step 9. Since the quantum yields show no wavelength dependence for the high air pressures employed in this study, reaction 10 is assumed to occur to collisionally relax $\text{A}_1^{v=w}$ molecules to common lower vibrational levels of the singlet state ($\text{A}_1^{v=m}$) from which either dissociation in step 11 or intersystem crossing in step 12 may occur to form the excited triplet species or possibly some other collisionally quenchable singlet state designated here as A_2 . The quenchable state A_2 may dissociate in reaction 13 at the lower pressures (below 375 torr of air), it may be deactivated in processes 15 and 16, or it may undergo internal conversion of the electronic energy to reform A_0 in reaction 14.

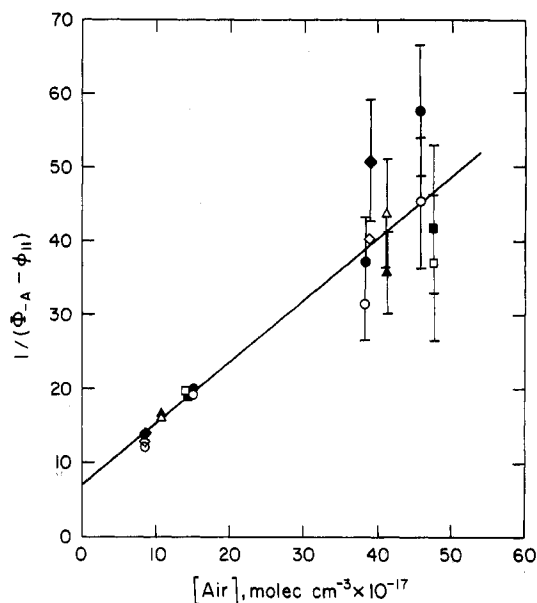


Figure 3. Plot of the function 18 of the text vs. concentration of air; symbols are as defined in Figure 2.

If one accepts this kinetic scheme and assumes that vibrational relaxation in reaction 10 is very fast for all air pressures employed, then relation 17 should hold, independent of wavelength. In the

$$\frac{1}{\Phi_{-\text{A}} - \phi_{11}} = \frac{k_{13} + k_{14}}{k_{13}\phi_{12}} + \frac{k_{15}[\text{O}_2] + k_{16}[\text{N}_2]}{k_{13}\phi_{12}} \quad (17)$$

majority of the experiments simulated air mixtures ($[\text{O}_2] = [\text{N}_2]/4$) were employed, and relation 18 applies to these cases.

$$\frac{1}{\Phi_{-\text{A}} - \phi_{11}} = \frac{k_{13} + k_{14}}{k_{13}\phi_{12}} + \frac{(k_{15} + 4k_{16})[\text{air}]}{5k_{13}\phi_{12}} \quad (18)$$

The value of $\phi_{11} = 0.0771 \pm 0.0022$ can be derived from the average of the high-pressure (greater than 370 torr) values of $\Phi_{-\text{A}}$ and Φ_{CO_2} . Since $\phi_{11} + \phi_{12} = 1.0$ according to the mechanism outlined, then $\phi_{12} = 0.923$. Using the derived experimental value of ϕ_{11} we have calculated the functions $1/(\Phi_{-\text{A}} - \phi_{11})$ and $1/(\Phi_{\text{CO}_2} - \phi_{11})$ for each experiment and plotted these vs. the concentrations of air in Figure 3. The data points for the experiments at lower air pressures (less than 48 torr) fit the theoretically expected linear dependence well. Data from the higher pressure runs show considerable scatter since the difference $\Phi_{-\text{A}} - \phi_{11}$ becomes inaccurate as $\Phi_{-\text{A}} \rightarrow \phi_{11}$. In view of the experimental error, the $\Phi_{-\text{A}} - \phi_{11}$ differences are meaningful only for data from experiments with air pressures below 160 torr. These data points are shown in Figure 3. From this plot one derives an intercept = 7.0 ± 2.4 which is equal in theory to $(k_{13} + k_{14})/(k_{13}\phi_{12})$, and a slope = $(8.3 \pm 0.8) \times 10^{-18} \text{ cm}^3 \text{ molecule}^{-1}$, equal in theory to $(k_{15} + 4k_{16})/(5k_{13}\phi_{12})$. Taking $\phi_{12} = 0.923$ we estimate $k_{13}/(k_{13} + k_{14}) \approx 0.16 \pm 0.05$ and $(k_{15} + 4k_{16})/k_{13} \approx (3.8 \pm 0.4) \times 10^{-17} \text{ cm}^3 \text{ molecule}^{-1}$.

The data from the experiments using pure O_2 mixtures with acetone are limited, but they can provide a measure of k_{15}/k_{13} . From the data at 25.3 torr of added O_2 we estimate $1/(\Phi_{-\text{A}} - \phi_{11}) \approx 27.1$ and 32.3 , taking ϕ_{11} and ϕ_{12} as before. These data and relation 17 give $k_{15}/k_{13} \approx 2.8 \times 10^{-17} \text{ cm}^3 \text{ molecule}^{-1}$. Coupling this with the data from the synthetic air mixtures gives $k_{16}/k_{13} \approx 2.5 \times 10^{-18} \text{ cm}^3 \text{ molecule}^{-1}$. It is clear, therefore, that a large fraction of the excited acetone molecules are quenched in air through collisions with oxygen molecules (>0.74) even though only 20% of the collisions are with molecular oxygen. The large efficiency of oxygen as a quencher of excited acetone molecules suggests that the A_2 state in the mechanism delineated above may be the lowest triplet state in acetone. If we assume this to be the case and accept the estimate of $k_{15} \approx 1.4 \times 10^{-11} \text{ cm}^3 \text{ molecule}^{-1} \text{ s}^{-1}$ as determined by Groh et al.,¹⁷ we may estimate from our data

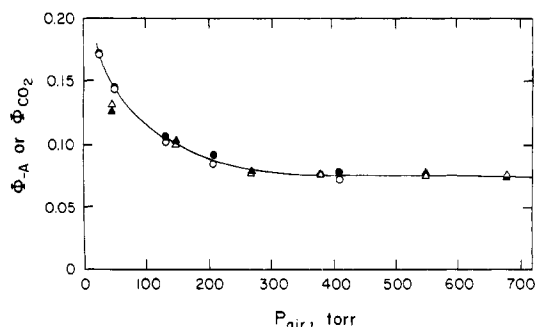


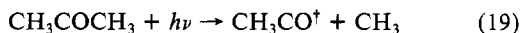
Figure 4. Quantum yields of acetone loss (closed symbols) and CO_2 formation (open symbols) vs. pressure of added air in experiments at several temperatures; excitation at 299 nm; temperature near 25 °C, circles; near 0 °C, triangles.

that $k_{13} \approx 5.0 \times 10^5 \text{ s}^{-1}$ at 25 °C. O'Neal and Larson¹⁸ suggested from their evaluation of available acetone photodecomposition data in the absence of O_2 that the activation energy for reaction 13, $E_{13} \approx 10 \pm 1 \text{ kcal mol}^{-1}$. Using this value, our data give a preexponential factor for reaction 13 of $A_{13} \approx 1.1 \times 10^{13} \text{ s}^{-1}$. This appears to be a reasonable magnitude for an apparent first-order decay constant for a molecule of the complexity of acetone at the pressures employed here. However, it is a factor of 10^2 larger than that derived by O'Neal and Larson.

Other definitive tests of the involvement of triplet acetone are not possible from the present data. Although this hypothesis is consistent with observed efficient O_2 quenching of the excited state in experiments at 25 °C, the negligible effect of temperature change on the quantum yields of acetone decomposition is inconsistent with this hypothesis if $E_{13} \approx 10 \text{ kcal mol}^{-1}$ as has been suggested. Compare in Figure 4 the quantum yield results from experiments at -1 and 25 °C using the 300-nm-band excitation. There is no significant temperature dependence to the excited acetone decomposition. Therefore, the interpretation of the nature of the quenchable electronic state of acetone remains ambiguous at this time.

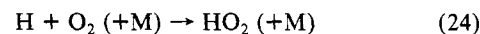
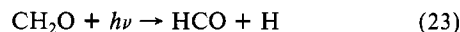
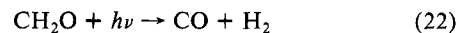
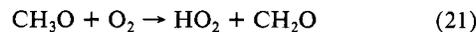
The alternative mechanism which involves a bimolecular chemical reaction between O_2 and excited acetone leading to the dissociation products seems unlikely, since oxygen gas quenches product formation rather than promotes reaction. It is possible that the unquenchable fraction of the acetone decomposition, which occurs with an efficiency limited by the magnitude of ϕ_{11} , involves a bimolecular O_2 -excited acetone reaction. However, this seems unlikely in view of the product distribution and its invariance with air pressure and temperature. These observations can be rationalized succinctly by assuming free-radical generation in the primary act as delineated in the following section.

Acetone photodecomposition in the absence of oxygen has been interpreted to involve the spontaneous decomposition of a fraction of the initial acetyl radicals which are formed in some vibrationally excited state:



The fraction α which represents $\phi_{19}/(\phi_{19} + \phi_1)$ varied from 0.07 at 313 nm to 0.22 at 254 nm.³ The product CO which is observed in the present experiments could conceivably have its origin in such a multiple-fragmentation, photochemical process (reaction 19) which would always be followed by reaction 20. This hypothesis seems improbable for several reasons: (a) The product yields do not exhibit a wavelength dependence; hence, the excess energy of the excited state observed in photolyses conducted in other studies at low pressure and in the absence of O_2 is apparently efficiently removed by collisions at the high gas pressures employed

here. (b) If CO were formed from acetyl radicals through a reaction such as reaction 20, the product data would follow the relation $\Phi_{\text{A}} = \Phi_{\text{CO}} + \Phi_{\text{CO}_2}$. This is not the case. (c) Furthermore, small amounts of hydrogen are observed among the products here, although its amounts could not be determined quantitatively with the chromatographic column and detector employed. We propose that the CO (and H_2) products originate in secondary reactions involving the photolysis of the initial CH_2O product formed in reactions 7, 8, and 21 which follow the CH_3 radical oxidation:



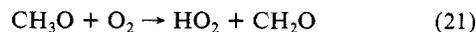
A separate set of experiments were designed to test this hypothesis. Since the amounts of H_2 formed in our experiments at relatively high oxygen pressures (Table I) could not be analyzed accurately by gas chromatography alone, the quantum yields of H_2 and CO were measured by using a combination of gas chromatography and mass spectrometry with pressures of oxygen between 5 and 10 torr and wavelengths of excitation of 280 and 300 nm. The measured ratios of $\Phi_{\text{H}_2}/\Phi_{\text{CO}}$, 0.40 and 0.20 at 280 and 300 nm, respectively, are identical within the experimental error with those predicted by using the primary quantum yield data of Calvert;¹⁹ for our conditions $\Phi_{\text{H}_2}/\Phi_{\text{CO}} = \phi_{22}/(\phi_{22} + \phi_{23}) = 0.44$ and 0.20 for 280 and 300 nm, respectively. The mechanism of H_2 and CO formation is further tested in the following sections.

Mechanistic Information from the Product Quantum Yields.

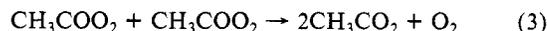
The major products for which quantitative analysis could be made in the present work include CO, CO_2 , CH_3OH , and CH_2O . All of these products are thought to arise from well-established reactions between O_2 and the primary fragmentation products of acetone photooxidation, namely, CH_3 and CH_3CO radicals. It can be shown from published rate constant data that H-atom abstraction reactions by these radicals, reacting with acetone or with products formed in the present system, cannot compete with reactions involving oxygen for our conditions ($[\text{CH}_3\text{COCH}_3] \approx 0.0007\text{--}0.07$ times the $[\text{O}_2]$; temperature ≤ 28 °C). In accord with this expectation, no product CH_4 or CH_3CHO was observed. Therefore, for our conditions, the only important reactions of the CH_3 and CH_3CO radicals are the following:



Subsequent reactions of these peroxy radicals must account for the observed products. For the CH_3O_2 radical the established reactions 6 and 7 are expected to occur. At the high $[\text{O}_2]$ employed here, the major reaction of the CH_3O radical formed in reaction 6 will be reaction 21 with O_2 :



Similar reactions between peroxyacetyl radicals must occur as well, but in this case only one reactive channel is expected, since no analogue to reaction 7 of the CH_3O_2 radical can exist for the CH_3COO_2 species.



In theory the $\text{CH}_3\text{O}_2\text{--CH}_3\text{COO}_2$ interactions could lead to two pathways analogous to the $\text{CH}_3\text{O}_2\text{--CH}_3\text{O}_2$ reactions 6 and 7 as has been discussed:

(17) H. J. Groh, Jr., G. W. Luckey, and W. A. Noyes, Jr., *J. Chem. Phys.*, **21**, 115 (1953).

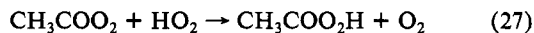
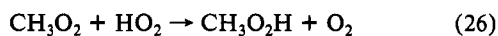
(18) H. E. O'Neal and C. W. Larson, *J. Phys. Chem.*, **73**, 1011 (1969).

(19) J. G. Calvert, "The Homogeneous Chemistry of Formaldehyde Generation and Destruction Within the Atmosphere", Report No. FAA-EE-80-20, Proceedings of the NATO Advanced Study Institute on Atmospheric Ozone, U.S. Department of Transportation, FAA, Office of Environment and Energy, High Altitude Program, Washington, DC, 1980, pp 153-90.



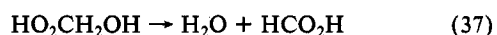
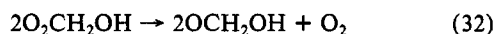
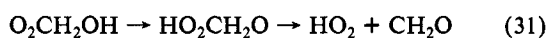
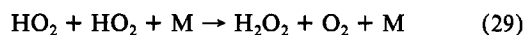
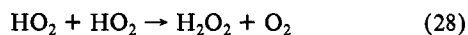
Although acetic acid was observed as a minor product ($0.001 < \Phi < 0.01$), the equality $\Phi_{-A} = \Phi_{\text{CO}_2}$ demands that reaction 5 be unimportant compared to reaction 4.

The HO_2 radicals formed in reaction 21 will also react with CH_3O_2 radicals, and in principle, CH_3COO_2 may react in an analogous fashion:

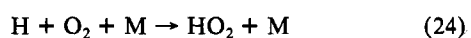
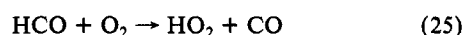
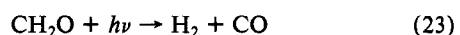


There is no experimental evidence for peroxyacetic acid among the products although its decomposition to CO_2 and other products during analysis could have masked its transient presence in these experiments. Either the unimportance of reaction 27 or possibly the decay of $\text{CH}_3\text{COO}_2\text{H}$ to CO_2 and other products must be accepted to rationalize the observed equality, $\Phi_{\text{CO}_2} = \Phi_{-A}$. It is probable that $k_{27} \ll k_4$, and therefore we neglect pathway 27.

The HO_2 radicals formed in reaction 21 will also react via the well-known reactions 28 and 29 to form H_2O_2 ; formic acid and other products will be formed in reaction sequence 30–37 involving HO_2 reactions with CH_2O .



The product formaldehyde absorbs ultraviolet light in the employed wavelength region and the extinction coefficients are nearly the same as those for acetone. However, the quantum yields for decomposition are much larger: $\phi_{22} + \phi_{23} = 1.0$ in the air mixtures employed.



The apparent first-order photodecomposition rates for CH_2O in these mixtures are about 13 times larger than those for acetone in experiments using more than 375 torr of air. Obviously the contribution of CO from such a process can be significant.

If we use the estimates for the relative rate constants of reactions 6 and 7 ($k_7/k_6 = 1.32 \pm 0.16$ at 25°C)²⁰ and accept the constraint that CH_3O radicals formed in reaction 6 always react with O_2 in reaction 21, and that both the formic acid product and other sources of CH_2O are minor, then the theoretical relation 38 should

$$\Phi_{\text{CH}_3\text{OH}}/(\Phi_{\text{CH}_2\text{O}} + \Phi_{\text{CO}}) = k_7/(2k_6 + k_7) = 0.40 \pm 0.03 \text{ at } 25^\circ\text{C} \quad (38)$$

describe the results obtained in this work. This expectation is in reasonable accord with the product quantum yield data in Table I. The average of the 17 values from experiments at 25°C and at air pressures above 30 torr gives $\Phi_{\text{CH}_3\text{OH}}/(\Phi_{\text{CH}_2\text{O}} + \Phi_{\text{CO}}) \approx 0.45 \pm 0.10$. Excluding the data for 300 nm which appear to be more scattered than the other data, we find (from the remaining

TABLE II: Mechanism and Rate Constants Used in Simulations of Acetone Photooxidation at 25°C

reaction	rate constant, $\text{cm}^3 \text{molecule}^{-1} \text{s}^{-1}$	ref
(9) $\text{A}_0 + h\nu \rightarrow \text{A}_1^{v=w}$		
(10) $\text{A}_1^{v=w} + \text{M} \rightarrow \text{A}_1^{v=w} + \text{M}$	$0.0771(I_a)^c$	<i>a</i>
(11) $\text{A}_1^{v=w} \rightarrow \text{CH}_3 + \text{CH}_3\text{CO}$		
(12) $\text{A}_1^{v=w} \rightarrow \text{A}_2$	$0.923(I_a)^c$	<i>a</i>
(13) $\text{A}_2 \rightarrow \text{CH}_3\text{CO} + \text{CH}_3$	5.40×10^5	<i>a</i>
(14) $\text{A}_2 \rightarrow \text{A}_0$	2.94×10^6	<i>a</i>
(15) $\text{A}_2 + \text{O}_2 \rightarrow \text{A}_0 + \text{O}_2(^1\Delta_g, ^1\Sigma_g^+, ^3\Sigma_g^-)$	1.40×10^{-11}	17
(16) $\text{A}_2 + \text{N}_2 \rightarrow \text{A}_0 + \text{N}_2$	1.67×10^{-12}	<i>a</i>
(2) $\text{CH}_3 + \text{O}_2 (+\text{M}) \rightarrow \text{CH}_3\text{O}_2 (+\text{M})$	rapid	23
(1) $\text{CH}_3\text{CO} + \text{O}_2 (+\text{M}) \rightarrow \text{CH}_3\text{COO}_2 (+\text{M})$	rapid	24
(6) $2\text{CH}_3\text{O}_2 \rightarrow 2\text{CH}_3\text{O} + \text{O}_2$	1.17×10^{-13}	20
(7) $2\text{CH}_3\text{O}_2 \rightarrow \text{CH}_2\text{O} + \text{CH}_3\text{OH} + \text{O}_2$	2.17×10^{-13}	20
(21) $\text{CH}_3\text{O} + \text{O}_2 \rightarrow \text{CH}_2\text{O} + \text{HO}_2$	1.48×10^{-15}	24
(41) $2\text{CH}_3\text{O} \rightarrow \text{CH}_2\text{O} + \text{CH}_3\text{OH}$	6.3×10^{-11}	25, 26
(42) $\text{CH}_3\text{O} + \text{HO}_2 \rightarrow \text{CH}_3\text{OH} + \text{O}_2$	3.2×10^{-11}	<i>b</i>
$\text{CH}_3\text{O} + \text{CH}_3\text{COCH}_3 \rightarrow \text{CH}_3\text{OH} + \text{CH}_2\text{COCH}_3$	1.2×10^{-18}	27
(40) $\text{CH}_3\text{O} + \text{CH}_2\text{O} \rightarrow \text{CH}_2\text{OH} + \text{HCO}$	3.09×10^{-16}	21, 22
(3) $2\text{CH}_3\text{COO}_2 \rightarrow 2\text{CH}_3\text{CO} + \text{O}_2$	1.30×10^{-15}	28
(4) $\text{CH}_3\text{O}_2 + \text{CH}_3\text{COO}_2 \rightarrow \text{CH}_3\text{O} + \text{CH}_3\text{CO}_2 + \text{O}_2$	4.4×10^{-14}	29
(5) $\text{CH}_3\text{CO}_2 \rightarrow \text{CH}_3 + \text{CO}_2$	1.0×10^{13}	<i>b</i>
(26) $\text{HO}_2 + \text{CH}_3\text{O}_2 \rightarrow \text{CH}_3\text{O}_2\text{H} + \text{O}_2$	1.3×10^{-12}	20
(28) $2\text{HO}_2 \rightarrow \text{H}_2\text{O}_2 + \text{O}_2$	1.63×10^{-12}	23
(29) $2\text{HO}_2 + \text{M} \rightarrow \text{H}_2\text{O}_2 + \text{M} + \text{O}_2$	4.86×10^{-32}	23
(27) $\text{HO}_2 + \text{CH}_3\text{COO}_2 \rightarrow \text{CH}_3\text{COO}_2\text{H} + \text{O}_2$	small	<i>a</i>
(22) $\text{CH}_2\text{O} + h\nu \rightarrow \text{H} + \text{HCO}$	$I_a\phi_{22}^c$	19, 30, 31
(23) $\text{CH}_2\text{O} + h\nu \rightarrow \text{H}_2 + \text{CO}$	$I_a\phi_{23}^c$	19, 30, 31
(24) $\text{H} + \text{O}_2 + \text{M} \rightarrow \text{HO}_2 + \text{M}$	rapid	23
(25) $\text{HCO} + \text{O}_2 \rightarrow \text{HO}_2 + \text{CO}$	rapid	23
(30) $\text{HO}_2 + \text{CH}_2\text{O} \rightarrow \text{HO}_2\text{CH}_2\text{O} \rightarrow \text{O}_2\text{CH}_2\text{OH}$	1.7×10^{-14}	32
(31) $\text{O}_2\text{CH}_2\text{OH} \rightarrow \text{HO}_2\text{CH}_2\text{O} \rightarrow \text{HO}_2 + \text{CH}_2\text{O}$	1.5	32
(33) $\text{O}_2\text{CH}_2\text{OH} + \text{CH}_3\text{O}_2 \rightarrow \text{OCH}_2\text{OH} + \text{CH}_3\text{O} + \text{O}_2$	9.9×10^{-14}	<i>b</i>
(32) $2\text{O}_2\text{CH}_2\text{OH} \rightarrow 2\text{OCH}_2\text{OH} + \text{O}_2$	9.9×10^{-14}	32
(34) $\text{O}_2\text{CH}_2\text{OH} + \text{CH}_3\text{COO}_2 \rightarrow \text{OCH}_2\text{OH} + \text{CH}_3\text{CO}_2 + \text{O}_2$	9.9×10^{-14}	<i>b</i>
(35) $\text{OCH}_2\text{OH} + \text{O}_2 \rightarrow \text{HCO}_2\text{H} + \text{HO}_2$	1.49×10^{-14}	32
(36) $\text{HO}_2 + \text{O}_2\text{CH}_2\text{OH} \rightarrow \text{HO}_2\text{CH}_2\text{OH} + \text{O}_2$	1.3×10^{-12}	<i>b</i>

^a Estimate derived from present study. ^b Authors' estimates based upon analogous published rate information. ^c I_a in these rate expressions is the intensity of the light ($\text{quanta cm}^{-2} \text{s}^{-1}$) absorbed by the specific molecule (A_0 in eq 9 and 12; CH_2O in eq 22 and 23); these relations represent rates rather than rate constants.

14 data points) that $\Phi_{\text{CH}_3\text{OH}}/(\Phi_{\text{CH}_2\text{O}} + \Phi_{\text{CO}}) \approx 0.41 \pm 0.05$, in excellent accord with the theoretical expectation of 0.40 ± 0.03 for the proposed mechanism.

However, the apparent close agreement of the present data with relation 38 is perhaps somewhat fortuitous since the considerations given neglect both the CH_2O loss in the formic acid forming sequence 30–37 involving the HO_2 radical, and the formation of CH_2O from the $\text{O}_2\text{--CH}_3\text{O}$ reaction 21 which should follow reaction 4 between CH_3O_2 and CH_3COO_2 . A more accurate theoretical expression which corrects the deficiencies of relation 38 is the following:

$$k_7/(2k_6 + k_7) = \Phi_{\text{CH}_3\text{OH}}/(\Phi_{\text{CH}_2\text{O}} + \Phi_{\text{CO}} + \Phi_{\text{HCO}_2\text{H}} + \Phi_{\text{HO}_2\text{CH}_2\text{OH}} - \Phi_{\text{CH}_2\text{O}(4)}) \quad (39)$$

Accordingly, $\Phi_{\text{CH}_2\text{O}}$ represents the experimentally observed quantum yield of formaldehyde, and $\Phi_{\text{CH}_2\text{O}(4)}$ is the theoretical quantum yield of CH_2O formed in the sequence of reactions initiated by reaction 4. Only if $\Phi_{\text{HCO}_2\text{H}} + \Phi_{\text{HO}_2\text{CH}_2\text{OH}} = \Phi_{\text{CH}_2\text{O}(4)}$

(20) C. S. Kan, J. G. Calvert, and J. H. Shaw, *J. Phys. Chem.*, **84**, 3411 (1980).

TABLE III: Comparison of Experimental (E) and Computer-Simulated (S) Quantum Yields for the 3130-Å-Region Photolysis of Acetone at 25 °C and $P_A = 0.35$ torr

	quantum yields of products shown								
	acetone (loss)	CO ₂	CO	CH ₂ O	CH ₃ OH	HCO ₂ H	CH ₃ O ₂ H	H ₂ O ₂	
				$P_{\text{air}} = 745.4$ torr					
E	0.080	0.080	<i>a</i>	0.025	0.019	<i>a</i>	<i>a</i>	<i>a</i>	
S	0.080	0.080	0.024	0.022	0.026	0.0353	0.0301	0.0198	
				$P_{\text{air}} = 375.3$ torr					
E	0.078	0.076	0.017	0.024	0.018	<i>a</i>	<i>a</i>	<i>a</i>	
S	0.084	0.084	0.024	0.022	0.027	0.0383	0.0412	0.0178	
				$P_{\text{air}} = 141.1$ torr					
E	0.099	0.094	0.028	0.029	0.023	<i>a</i>	<i>a</i>	<i>a</i>	
S	0.096	0.096	0.025	0.025	0.031	0.0454	0.0476	0.0174	
				$P_{\text{air}} = 26.7$ torr					
E	0.160	0.149	0.036	0.036	0.032	<i>a</i>	<i>a</i>	<i>a</i>	
S	0.144	0.144	0.031	0.033	0.049	0.0768	0.0680	0.0207	

^aNot determined.

does relation 39 reduce to eq 38. Computer simulations of the chemical reactions which occur in this system (see next section) indeed suggest in theory that $\Phi_{\text{HCO}_2\text{H}} + \Phi_{\text{HO}_2\text{CH}_2\text{OH}} \approx \Phi_{\text{CH}_2\text{O}(4)}$. In simulations of experiments using radiation at the 313-nm region and 25 °C for the 26-torr run, $\Phi_{\text{HCO}_2\text{H}} + \Phi_{\text{HO}_2\text{CH}_2\text{OH}} = 0.11$ while $\Phi_{\text{CH}_2\text{O}(4)} = 0.07$; at 141 torr, these values are 0.06 and 0.05, respectively; at 375 torr they are 0.05 and 0.04, and at 745 torr they are 0.05 and 0.04, respectively. Therefore, the near agreement of the experimental data with relation 38 supports the mechanism outlined.

Data from experiments using the 280-, 290-, and 300-nm regions for excitation show an increase of product CH₃OH in experiments at the lowest pressures. Conceivably this "excess" CH₃OH could result from the occurrence of H-atom abstraction reactions of the CH₃O radical such as reaction 40 which may be



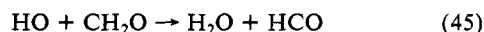
competitive with reaction 21 for these conditions. However, this explanation requires a value of $k_{40} \approx 1.7 \times 10^{-13} \text{ cm}^3 \text{ molecule}^{-1} \text{ s}^{-1}$ to match the CH₃OH data in simulations of the low [O₂] experiments. This value of k_{40} is several orders of magnitude greater than that derived from the combined data of Hoare and Wellington²¹ and Hecklen and Johnston.²² Hence, reaction 40 and the analogous slower reaction of CH₃O with CH₃COCH₃ appear to be unlikely sources of the additional CH₃OH observed in experiments at low [O₂]. Alternative sources are not obvious. Simulations show that other potential reactions such as reactions 41 and 42 are also very minor sources of CH₃OH.



The absorption coefficients of CH₃O₂H and H₂O₂ are much smaller than those of CH₃COCH₃ and CH₂O for the employed wavelength bands excitation. Therefore, although H₂O₂ and CH₃O₂H are theoretically expected to be major products of acetone photooxidation, their secondary photolyses



are probably of minor importance. However, to the extent that reactions 43 and 44 occur, it is likely that the resulting HO radicals will attack product CH₂O rather than reactant acetone since the rate coefficients for these reactions greatly favor CH₂O attack over reaction with CH₃COCH₃:



(21) D. E. Hoare and C. A. Wellington, "8th Symposium (International) on Combustion", Williams and Wilkins, Baltimore, MD, 1962, p 472.

(22) J. Hecklen and H. S. Johnston, *J. Am. Chem. Soc.*, **84**, 4030 (1962).

There is no evidence of a chain reaction in acetone photooxidation for our conditions, and the observed equality of quantum yields of acetone loss and CO₂ formation requires the unimportance of reaction 46. The net result of the minor occurrence of reactions 43 and 44 followed by reactions 45 and 25 should result in a small increase in the CO product quantum yield and a decrease in that of CH₂O. Neglecting this in our treatment does not alter any of the kinetic arguments given; if the photolyses of CH₃O₂H and H₂O₂ occur measurably, then a small portion of the total CH₂O decrease currently attributed to the photolysis of CH₂O would be reapportioned to reactions 43–45 and 25.

Computer Simulations of the Chemistry of Acetone Photooxidation in Air-Rich Mixtures. It is instructive to incorporate all of the chemical reactions and known rate coefficients (summarized in Table II) in a computer simulation of the experimental system and to attempt to test observed product quantum yields. We have picked four representative 313-nm experiments over the employed range of pressures to verify the general compatibility of the theory and experiment. The experimental and theoretical quantum yields of the observed products are compared in Table III. It can be seen that there is reasonably good agreement between experiment and simulations based upon the proposed mechanism, and some confidence is gained in its major mechanistic features.

The carbon balances in the runs at 25 °C (those at the lower [O₂] for which CO could be analyzed) give an average value of $61 \pm 5\%$ of the total carbon in the reacted acetone. In the simulations made here the theoretical mass balances, including only the products observed experimentally, show a very similar range of values: $58 \pm 4\%$ of the carbon is accounted for in these products. Obviously the data are in good accord with the suggested mechanism for product formation.

In summary, the simulation results are consistent with the general features of the reaction mechanism outlined. Acetone

(23) NASA Panel for Data Evaluation, No. 6, W. B. DeMore, M. J. Molina, R. T. Watson, D. M. Golden, R. F. Hampton, M. J. Kurylo, C. J. Howard, and A. R. Ravishankara, *JPL Publ.*, No. 82-62 (1983).

(24) CODATA Task Group on Gas Phase Chemical Kinetics, D. L. Baulch, R. A. Cox, R. F. Hampson, J. A. Kerr, J. Troe, and R. T. Watson, *J. Phys. Chem. Ref. Data*, **11**, 327 (1982).

(25) M. J. Yee Quee and J. C. J. Thynne, *Trans. Faraday Soc.*, **62**, 3154 (1966).

(26) M. J. H. Wijnen, *J. Chem. Phys.*, **28**, 271 (1958).

(27) Based on the rate constant for the analogous reaction, $\text{CF}_3 + \text{CH}_3\text{COCH}_3 \rightarrow \text{CF}_3\text{H} + \text{CH}_2\text{COCH}_3$; see J. A. Kerr and S. J. Moss, "Handbook of Bimolecular and Termolecular Gas Reactions", Vol. 1, CRC Press, Boca Raton, FL, 1981.

(28) This rate constant was assumed to be equal to that for the analogous *i*-C₃H₇O₂ reaction, L. J. Kirsch, D. A. Parkes, D. J. Waddington, and A. Woolley, *J. Chem. Soc., Faraday Trans. 1*, **74**, 2293 (1978).

(29) Authors' estimate based upon $k = 2(k_{2\text{CH}_3\text{O}_2}k_{2\text{-C}_3\text{H}_7\text{O}_2})^{1/2}$.

(30) A. Horowitz and J. G. Calvert, *Int. J. Chem. Kinet.*, **10**, 805 (1978).

(31) G. K. Moortgat and P. Warneck, *J. Chem. Phys.*, **70**, 3639 (1979).

(32) F. Su, J. G. Calvert, and J. H. Shaw, *J. Phys. Chem.*, **83**, 3185 (1979).

TABLE IV: Apparent First-Order Photodissociation Rate Constants for Acetone in the Troposphere Near Sea Level Compared with CH₂O and CH₃CHO data

solar zenith angle, deg	rate constant, s ⁻¹		
	10 ⁶ k- (CH ₃ COCH ₃)	10 ⁵ k- (CH ₂ O) ^a	10 ⁶ k- (CH ₃ CHO) ^a
0	1.17	6.0	3.5
20	1.08	5.8	3.4
40	0.785	4.7	2.2
60	0.365	2.7	1.0
78	0.057	0.6	0.13
86	0.016	0.1	

^aThese represent total decomposition rates which are the sum of several processes; data for CH₂O are from ref 29-31; data for CH₃C-HO are from ref 35 and 36.

photodecomposition in air shows a pressure-sensitive generation of methyl and acetyl radicals which, for a given pressure, is relatively independent of the band of excitation wavelengths (280-313 nm) and temperature (-1 to 28 °C).

Estimation of the Theoretical First-Order Photolysis Rate Constants for Acetone in the Troposphere. All of the acetone photodecomposition quantum yields observed in this work can be accurately summarized through the empirical equation 47 derived

$$\Phi_{-A} = \Phi_{\text{CO}_2} = 0.0766 + 0.09415e^{-[\text{air}]/(3.222 \times 10^{18})} \quad (47)$$

from a least-squares fit of the data. Relation 47 was selected for its simplified formulation. The representation of $\Phi_{-A} = a + b/(c + d[\text{air}])$, expected in theory from the proposed mechanism, also fits the data well but requires a greater number of constants. The concentration of air, [air], is in units of molecules cm⁻³. Equation 47 can be combined with solar irradiance and acetone absorption coefficient estimates to calculate the apparent first-order photo-

chemical decay constants for various solar zenith angles and altitudes within the troposphere.³³ However, we may use the representative theoretical solar irradiances for the lower troposphere, published by Demerjian et al.,³⁴ and our measured absorption coefficient data for acetone, to estimate the first-order acetone photodissociation constant for various solar zenith angles at a location near sea level. These results are summarized in Table IV, where they can be compared with the photolysis constants for CH₂O and CH₃CHO. It is apparent that the photodissociation of acetone in the lower troposphere is much smaller than that for CH₂O and CH₃CHO. The photodissociation lifetimes of the three compounds (1/k_{dissoc}) for 40° solar zenith angle are 14.8 days for CH₃COCH₃, 5.9 h for CH₂O, and 5.3 days for CH₃CHO. Since the rate constant for HO attack on CH₃COCH₃ is also much smaller than those for CH₂O and CH₃CHO, it is readily seen why the tropospheric [CH₃COCH₃] can build up to significant levels.

Acknowledgment. This work was supported by an Interagency Agreement (DW4990319-01-1) between the Environmental Protection Agency and the National Science Foundation. We thank Dr. William R. Stockwell of NCAR for his help in computer simulation of the acetone photooxidation results and Professor J. Alistair Kerr of the University of Birmingham for his evaluation of rate data used in the simulations.

Registry No. CH₃COCH₃, 67-64-1; CH₃OH, 67-56-1; CH₂O, 50-00-0; CO₂, 124-38-9; CO, 630-08-0.

(33) Dr. Robert Chatfield of the National Center for Atmospheric Research is working with us in carrying out these calculations which will be published separately.

(34) K. K. Demerjian, K. L. Schere, and J. T. Peterson, *Adv. Environ. Sci. Technol.*, **10**, 369 (1980).

(35) A. Horowitz, C. J. Kershner, and J. G. Calvert, *J. Phys. Chem.*, **86**, 3094 (1982).

(36) A. Horowitz and J. G. Calvert, *J. Phys. Chem.* **86**, 3105 (1982).

A Classical plus Tunneling Model for Unimolecular Reaction Dynamics: The HNC → HCN Isomerization

Boyd A. Waite

Department of Chemistry, United States Naval Academy, Annapolis, Maryland 21401
(Received: March 12, 1984)

A classical plus tunneling model is developed for describing mode-specific behavior in unimolecular reaction dynamics. Initial conditions are chosen to correspond to various bond-specific preparations, the system then evolving according to the full classical Hamiltonian. At barrier turning points, the trajectories are stopped, and local tunneling probabilities are computed and averaged over to yield a survival probability as a function of time. The HNC-HCN unimolecular isomerization reaction is studied with a potential energy surface of Pearson et al. Results indicate a fair amount of mode specificity at low energies, but much less mode specificity at energies above the classical threshold for the reaction. A phenomenological analysis of mode specificity in unimolecular reactions is also presented, yielding results in qualitative agreement with the trajectory calculations.

I. Introduction

Various experimental and theoretical aspects of unimolecular reaction dynamics have recently been reviewed.¹⁻³ Previous work by this author⁴⁻⁷ and others⁸ has focused on the question of mode

specificity in unimolecular reaction dynamics. Central to this idea is the possibility of controlling the rate of unimolecular reaction by preparing the reactant in a specific energy configuration, e.g., via overtone excitation^{9,10} of a particular bond or mode by using a finely tunable laser. For the process



- (1) K. A. Holbrook, *Chem. Soc. Rev.*, **12**, 163 (1983).
 (2) W. L. Hase in "Potential Energy Surfaces and Dynamics Calculations", ACS Symp. Ser., D. G. Truhlar, Ed., Plenum, New York, 1981, p 1.
 (3) C. E. Dykstra, *Annu. Rev. Phys. Chem.*, **32**, 25 (1981).
 (4) B. A. Waite and W. H. Miller, *J. Chem. Phys.*, **73**, 3713 (1980).
 (5) B. A. Waite and W. H. Miller, *J. Chem. Phys.*, **74**, 3910 (1981).
 (6) B. A. Waite and W. H. Miller, *J. Chem. Phys.*, **76**, 2412 (1982).
 (7) B. A. Waite, S. K. Gray, and W. H. Miller, *J. Chem. Phys.*, **78**, 259 (1983).

(8) W. P. Reinhardt, *Annu. Rev. Phys. Chem.*, **33**, 223 (1982).

(9) See, for example, "Advances in Laser Chemistry", A. H. Zewail, Ed., Springer, New York, 1978.

(10) See, for example, "Laser-Induced Processes in Molecules", K. L. Kompa and S. D. Smith, Ed., Springer, New York, 1979.